Real-time digital design for an optical coherence tomography acquisition and processing system

Tyler S. Ralston[a,b], Jose A. Mayen[a,b], Dan Marks[a,b], and Stephen A. Boppart[a,b,c,*]

[a]Beckman Institute for Advanced Science and Technology
University of Illinois Urbana-Champaign 405 N. Mathews Ave. Urbana, IL 61801
[b]Department of Electrical and Computer Engineering
University of Illinois Urbana-Champaign, 1406 W. Green St. Urbana, IL 61801
[c]Bioengineering Program, College of Medicine
University of Illinois Urbana-Champaign

ABSTRACT

We present a real-time, multi-dimensional, digital, optical coherence tomography (OCT) acquisition and imaging system. The system consists of conventional OCT optics, a rapid scanning optical delay (RSOD) line to support fast data acquisition rates, and a high-speed A/D converter for sampling the interference waveforms. A 1M-gate Virtex-II field programmable gate array (FPGA) is designed to perform digital down conversion. This is analogous to demodulating and low-pass filtering the continuous time signal. The system creates in-phase and quadrature-phase components using a tunable quadrature mixer. Multistage polyphase finite impulse response (FIR) filtering and down sampling is used to remove unneeded high frequencies. A floating-point digital signal processor (DSP) computes the magnitude and phase shifts. The data is read by a host machine and displayed on screen at real-time rates commensurate with the data acquisition rate. This system offers flexible acquisition and processing parameters for a wide range of multi-dimensional optical microscopy techniques.

Keywords: digital signal processing, optical coherence tomography, Doppler, spectroscopic, real-time.

INTRODUCTION

Optical coherence tomography is an emerging, near-infrared imaging and microscopy technique capable of micrometer-scale resolutions within living biological samples [1]. Being a noninvasive imaging technique that has resolution on the order of several microns, OCT has been demonstrated in a wide range of medical, surgical, and biological applications [2].

Doppler OCT, a technique analogous to Doppler ultrasound, has been used to acquire image-based data of fluid flow profiles and make quantitative measurements of flow velocities. Doppler OCT forms images corresponding to interference frequency variations. Related literature details Doppler OCT theory and implementations [3-11]. Previously, Doppler OCT images were generated offline due to the delay of the intense computation [3,4]. For instance, ninety-six thousand 32-point fast Fourier transforms, one for each pixel, were computed for the frequency centroid data. From the frequency centroid data and known Doppler shifts, these computations required 10 s on a 200MHz host computer [3]. Newer solutions for computing Doppler OCT images no longer required the use of a short-time Fourier transform (STFT) [5-11]. A phase-resolved method allows for detection of very slow velocities such as blood flow in capillaries [6,7]. In this method, the instantaneous phase from the in-phase and quadrature-phase data of each sample in an axial scan determines the Doppler frequency variations. Then, another axial scan is taken at the same lateral position and the instantaneous phase recalculated. The ratio of the difference between the adjacent instantaneous phase values to the axial scan period determines the instantaneous frequency produced by the scatterers at each interval along the axial scan. This technique assumes that adjacent axial scans contain the same scatterers. Phase-resolved velocity images have significantly shorter data acquisition times

* For correspondence with Dr. Stephen A. Boppart email: boppart@uiuc.edu phone: (217) 244-7479

Three-Dimensional and Multidimensional Microscopy: Image Acquisition and Processing XI,
edited by Jose-Angel Conchello, Carol J. Cogswell, Tony Wilson, Proc. of SPIE Vol. 5324
(SPIE, Bellingham, WA, 2004) · 1605-7422/04/$15 · doi: 10.1117/12.527829

than the STFT method with equivalent sensitivity. For example, averaging eight axial scans per image column, velocity sensitivities as low as 10 μm/s are attained [6]. A similar method is employed in our hardware, which is described in the next section.

Implementing a digital autocorrelator or an optical Hilbert transform are two additional solutions for finding a real-time solution for Doppler OCT [8,9]. Corresponding research has shown that data processing is commensurate with acquisition times. Another common solution to the computational needs for real-time Doppler OCT imaging is to perform critical structural and velocity calculations using a digital signal processor [10,11]. This processor, which is tailored to perform real-time signal computations, can calculate structure and velocity from in-phase and quadrature-phase data. A drawback to some systems is the inability to process data equivalently at multiple different Doppler frequencies as a result of different optical delay line configurations [11].

With the emergence of broad bandwidth light sources, techniques in spectroscopic OCT have been developed for displaying images with wavelength reflectance resolution [12,13]. Spectroscopic OCT has the ability to enhance the image contrast, which may be notably applicable to tissue pathology for differentiation of tissues having unique spectroscopic properties [14]. The techniques employed by each of these papers is to perform either a STFT or a Morlet wavelet transform, find a center of mass, and map the center of mass and the centroid shift to the corresponding color space, saturation and hue, respectively, holding luminance constant. Outlined in the next section is a technique to acquire spectroscopic information at a specific single frequency, within a certain bandwidth, for multiple wavelengths. In essence, our system enables spectral calculations that are analogous to the STFT or the Morlet wavelet transform.

Furthermore, a variety of high-speed, fast acquisition OCT systems have been tailored for multiple functions such as Doppler OCT, and polarization sensitive OCT [15-17]. For example, it has been shown that a real-time multi-functional system can simultaneously produce images of structure, birefringence, and blood flow [15]. Medical and biological imaging may be dependent upon transient events, for which real-time acquisition and processing are necessary [16]. A system utilizing commercial Doppler ultrasound techniques is able to attain real-time Doppler, velocity variance, Doppler spectrum, and power Doppler at a rate of 32 frames per second and 250X512 pixels per image [17].

Methods to create a stable interference fringe carrier frequency have been a topic of concern among recent literature [18]. For example, in one such method, spectrally modulated sidelobes could be suppressed by signal processing of the source's spectrum. Among the limitations of current systems, one is that of fully utilizing an optical delay line which has a modulation pattern inherent in its design.

It is one of our goals in building this system to create a system capable of dynamically demodulating an interferogram to fit unique modulation patterns created by an optical delay line. Thus, our design choice of a quadrature amplitude demodulator is appropriate for this task. Dynamic demodulation may be done by adjusting the local oscillator during the mixing phase of the digital demodulation to compensate for Doppler shifts induced by the changing velocities of the delay line, whether it is a polygonal or a resonant scanner.

Furthermore, the choice of a quadrature mixer in combination with FIR filters allows for the ability to image different frequency selections of the imaging spectrum, thus producing the ability to produce the spectroscopic characteristics of a sample.

HARDWARE AND METHODOLOGY

1. Optical system

Our OCT system is implemented using a low-coherence light source, ultra-high numerical aperture (UHNA) fiber, a Michelson interferometer, and a rapid scanning optical delay (RSOD) line that includes a resonant scanner. Figure 1 illustrates the primary hardware configuration for generating, acquiring, and processing interference patterns.

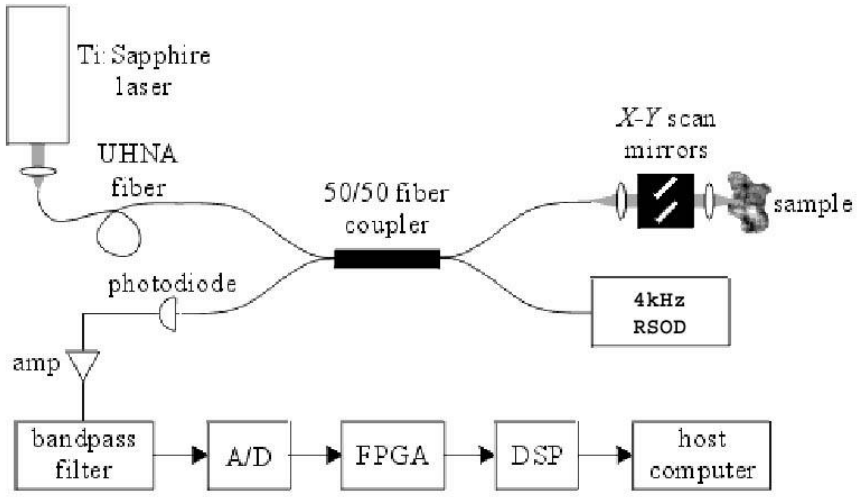

Figure 1. Complete setup for the fast scanning OCT system used for primary testing of FPGA, DSP, and host computer configuration and performances indices.

The RSOD is a Fourier-domain delay line that allows for adjustable phase and group velocities [19]. The phase velocity produced by the RSOD determines the modulation frequency at the output of the interferometer. The RSOD is driven with a 4kHz sine wave generated by the FPGA. The choice of an RSOD was based on the desire to scan fast and to test the adjustable demodulation of our digital design. It is important to note that although the maximum scan rate is usually desired, an increase in speed requires a proportional increase in optical power to maintain the same SNR [20]. Increases in optical power are possible with mode-locked laser sources such as the one used here, however laser safety limits for tissue injury can be reached, particularly if the scanning beam remains stationary on the specimen under investigation.

As depicted in Figure 2, light travels along the reference path and then is dispersed by a grating. The Fourier spectrum of this light is obtained one focal distance (f) away from a lens. Phase shifts are induced in the frequency domain by reflecting light off of a pivoting mirror. The inverse Fourier transform of the returning light is obtained one focal distance away from the lens as it returns. As a result, the phase shifts induced by the mirror become time shifts (delays).

The RSOD-induced Doppler frequency is given by

$$f_{\mathrm{RSOD}} = \frac{2x_0}{\alpha}\frac{\mathrm{d}\alpha(t)}{\mathrm{d}t}.$$

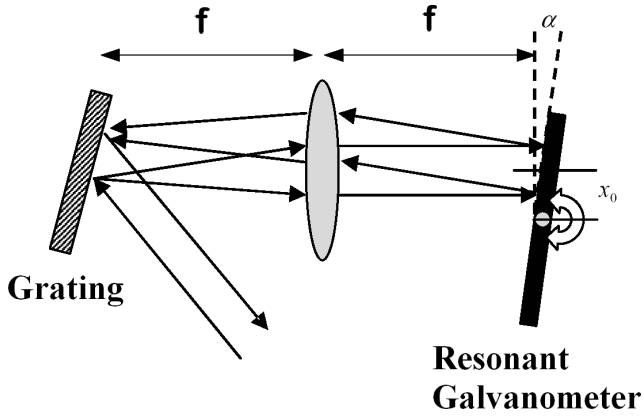

Figure 2. Schematic of an RSOD as used for a Fourier-domain delay-line.

Another RSOD compatible with the system is one that uses a polygonal scanner [21]. It consists of a Fourier-domain delay line that is scalable to higher speed without limiting the mirror size, since the delay element is a rotating polygonal mirror array. This device is typically linear in group delay, and as with other Fourier-domain delay lines, its phase delay (and hence modulation frequency) can be adjusted independently. Due to the geometry of the polygon, there exist nonlinearities in the phase delay, which cause the modulation signal to be chirped. Since the chirp in the modulation frequency is linear, it is straightforward to compensate for it digitally so that this delay line can be used for phase-sensitive applications such as Doppler and Spectroscopic OCT. To compensate for the chirp, the local oscillator of the demodulator would be moved linearly to track the Doppler frequency per scan line.

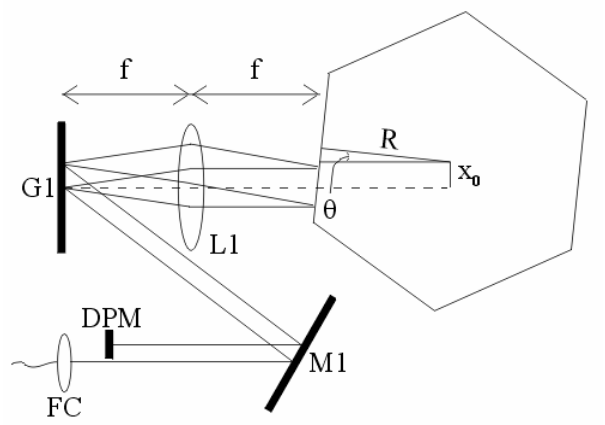

Figure 3. Functional schematic of a polygonal mirror array as used for a Fourier-domain delay line. DPM, double-pass mirror; FC, fiber collimator; G1, grating; L1 achromatic lens; M1, steering mirror.

The phase velocity determines the modulation frequency for this device:

$$f_{\mathrm{mod}} = \frac{1}{\lambda_0}\frac{\partial l_p}{\partial t} \approx \frac{4\omega}{\lambda_0}\left(x_0 - R\theta\right),$$

where ω is the mirror's rotational velocity. The association of the $R\theta$ term with f_{mod} is that f_{mod} varies over the scan, introducing a chirp to the detection signal.

2. Electronics and digital system

2.1. Quadrature mixer for digital down conversion

The interference waveform from a photodetector (Model 1801, New Focus, Inc.) is conditioned to match the dynamic range of the A/D converter. After conversion from optical interference to electrical current, a differential amplifier and bandpass filter condition the signal to peak at 1 V.

Through the implementation of a digital system, we are able to attain versatility not yet achievable through standard methods of OCT acquisition and processing. The digital system is able to acquire the data at a fast enough rate such that the Doppler frequency need not be demodulated in an analog fashion before sampling. By implementing an FPGA, the image data can be processed in real time to produce desired images for structural, Doppler, or spectroscopic data. A PCI module carrier board (HEPC8, Hunt Engineering, UK) performs as the primary communication between the FPGA module (HERON-IO2V2, Hunt Engineering, UK) and the DSP module (HERON 4, Hunt Engineering, UK) [22-24]. The carrier board contains 50MHz, 32 bit wide by 512 deep first-in-first-out (FIFO) data queues between the each module as well as one FIFO that communicates through the PCI bus to the host computer. The FPGA module contains a Virtex II FPGA with connections to 2 channels of 105MHz 12 bit A/D and 2 channels of 125MHz 14 bit D/A. Our system makes use of 2 D/A's for the galvanometers and 1 A/D for the interference data. The DSP module is fitted with a Texas Instruments C6701 processing module operating at 132 MHz.

We chose to implement our system with a 50MHz acquisition clock. A high clock rate is good for an FPGA because the clock rate is directly proportional to the amount of the completed computation. This allows for accurate retrieval of the Doppler frequencies through oversampling as well as the ability to do multiple simultaneous computations quickly. By designing hardware capable of processing our data and controlling the acquisition process, we can utilize all the data as it comes in at 50MHz. Therefore, the hardware is set up so that data flows through the system separately from the instructions, a Harvard Architecture. A Harvard Architecture maximizes processing power by maintaining two separate memory bus structures, program and data, for full-speed execution. This multiple bus structure allows data and instruction reading to overlap. Instructions do not hinder data transfers between two spaces. Furthermore, this design provides liberty to parallelize computations at the expense of available resources. Therefore, to design the hardware data path efficiently, we choose certain parameters for each of our components that, we believe, give the best overall benefit. Adjustable parameters in the data path include modulation resolution, FIR filter design, tap length, and decimation ratios. Figure 4 diagrams the critical data path in the FPGA.

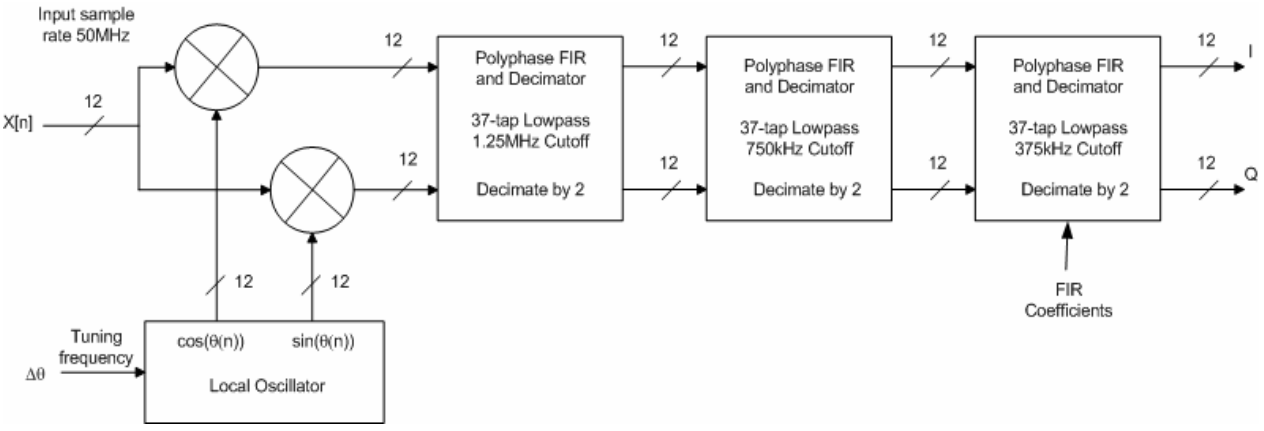

Figure 4. Critical data path through the FPGA.

The quadrature demodulation is implemented using a numerically controlled oscillator logic core (Xilinx LogiCore v.4.1) [25]. This hardware, as seen in Figure 5, operates using a sine function look-up table having two read ports, one 90 degrees out of phase with the other, a phase increment register, and a phase accumulator. The

look-up table has an input port to assign a phase increment within the table. This serves to adjust the demodulation in congruence with the Doppler frequency. The resolution of the system is designed for accuracy up to 1536Hz apart. In our setup, this provides 600 μm/s velocity resolution yet allows enough room for the FIR filters on the chip and maintains a reasonable amount of precision for tuning our Doppler frequency.

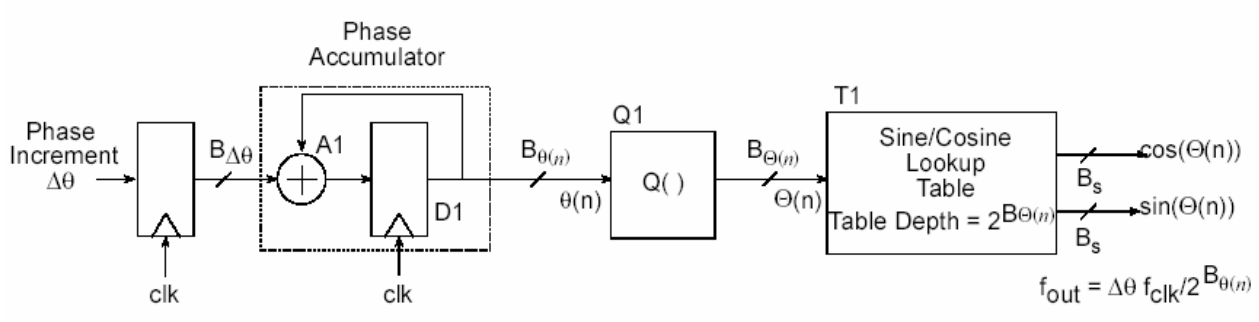

Figure 5. Numerically controlled oscillator used for quadrature mixing. A1 and D1, integrator; Q1, quantizer; T1, look-up table; θ(n), high precision phase angle;Θ(n), lower precision phase angle.

The ability to dynamically control the demodulation frequency allows us to compensation for delay line effects introduced by the RSOD and the polygonal scanner, as well as other any other delay lines which introduces specific modulation patterns. To compensate for a resonant RSOD's nonlinear, sinusoidal modulation, we can demodulate 90 degrees out of phase of the position, since the derivative of the position is the velocity of the RSOD. This is possible since the RSOD control signal is generated by the FPGA. The phase increment register of the digital down converter is just assigned a constant delay of the driving sinusoid input. Figure 6 shows a generalized waveform for the local oscillator, the phase increment and the RSOD position.

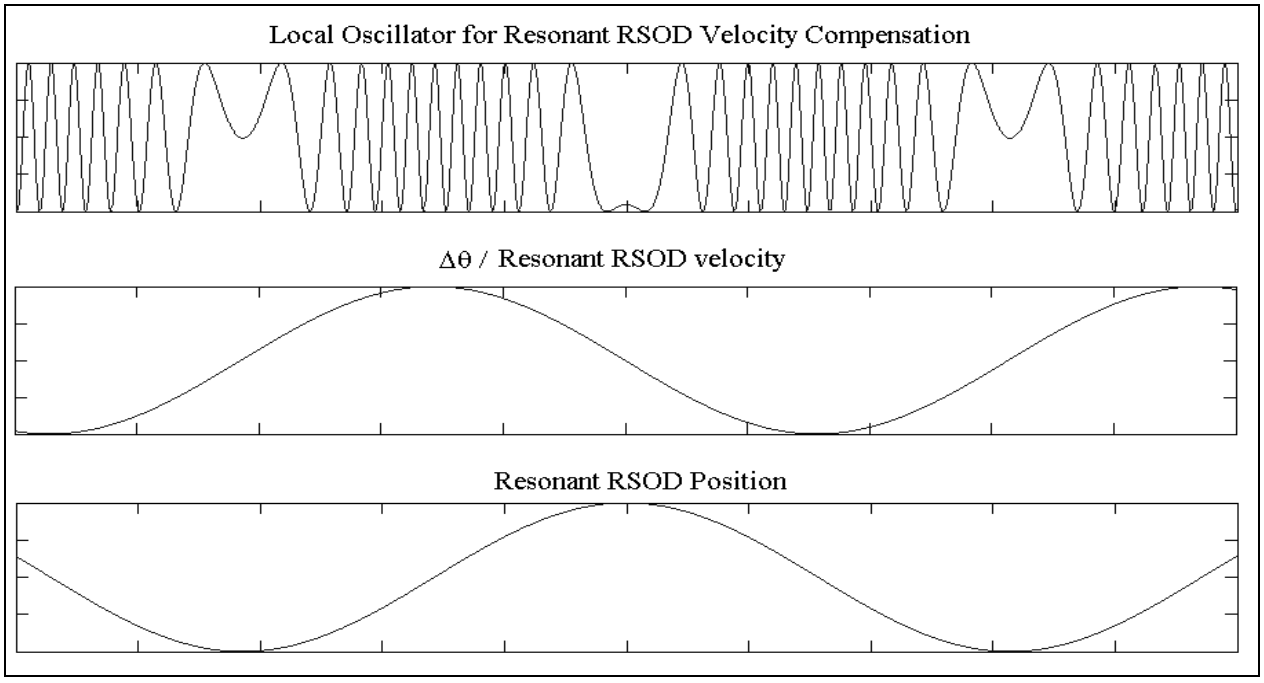

Figure 6. Generalized waveform of numerically controlled oscillator, phase increment, and resonant RSOD position.

To compensate for the polygonal scanner's chirped modulation pattern, the phase increment of the demodulator is assigned from the value of a register, which is incremented by a counter during a scan line. At the end of the line the register is reset. The effect is a local oscillator that tracks the modulation frequency for demodulation. To attain the increment, the system must first be calibrated by imaging a flat reflective object (i.e. coverslip).

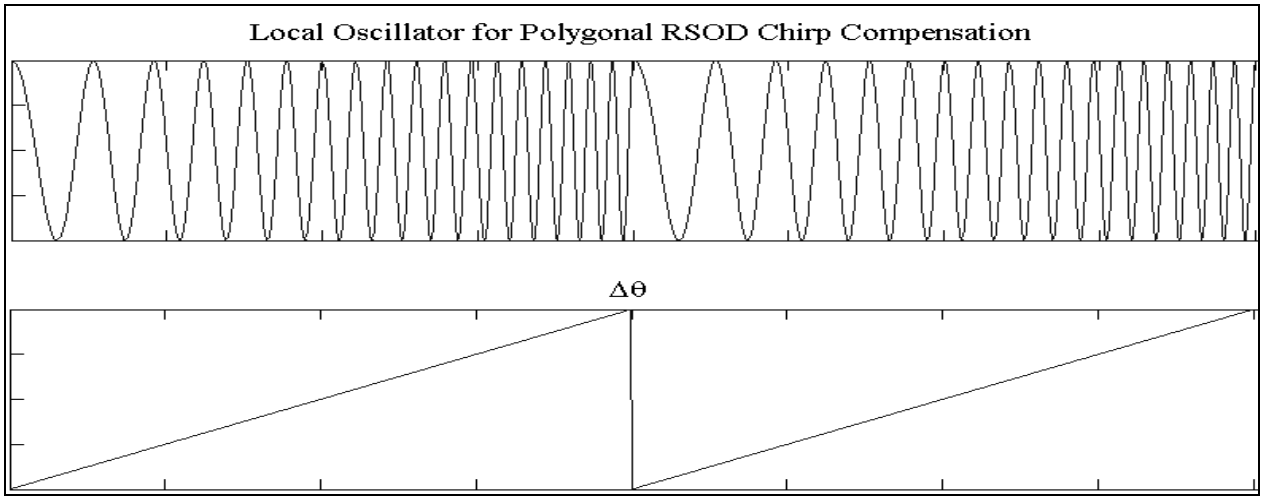

Figure 7. Generalized waveform of numerically controlled oscillator and phase increment of polygonal RSOD.

For the approach of attaining spectroscopic images, frequency specific information can be attained though the use of narrow FIR lowpass filters in conjunction with demodulating at the wavelength's corresponding baseband demodulation frequency. In this method, multiple images are attained by demodulating over a range of frequencies, ω_j, determined by the available bandwidth of the laser source. Each image represents the backscattered wavelength corresponding to its demodulation frequency. Each pixel within an image demodulated at frequency ω_j has a corresponding amplitude, $A_{x,z}(\omega_j)$. To display the spectroscopic data in an image, a multidimensional map similar to the referenced text can be used [12]. The saturation is represented per pixel by $T_{x,z} = \sum_j A_{x,z}(\omega_j)$, hue is represented by center of mass per pixel, $\Omega_C(x,z) = \sum_j A_{x,z}(\omega_j) \cdot \omega_j$, and the luminance is held constant.

2.2. Finite impulse response (FIR) lowpass filter for digital down conversion

Lowpass filtering is essential in down conversion for removing the false frequencies created during quadrature mixing. It is our choice to design the lowpass filters as FIR filters due to their stability and linearity in phase, which is necessary for accurate Doppler retrieval. For good resource utilization and reconfigurability, the lowpass filtering is done with multi-stage, polyphase FIR filters interleaved with decimation.

Dividing the lowpass filtering into three stages produces a better overall filtering result. Decimation ratios between each stage allow the following stages to use less hardware per cycle, thus increasing our subsequence number of FIR taps. This is because each FIR filter is set up in hardware as polyphase computation. In this multirate configuration, the convolution computations are parallelized. The first stage is typically a wider filter than the following filters. Specifically, the first stage must have multiply hardware for each coefficient, but the following filters can operate with less multiply hardware due to the sample rate decimation. Therefore, starting with shorter (wider) filters and then progressing toward longer (narrower) filters is optimal. In our default system, the first filter

has a pass band cut off at 1.25MHz, the second at 750kHz, and the final at 375kHz. This allows for a smooth transition band, which is adequate for down conversion of a wide range of Doppler frequencies.

After each of the FIR filters, the signal is decimated by a factor of two, which yields an overall decimation of eight. As a default setup, the stages are all lowpass filters designed using the Remez Exchange algorithm to create Parks-McClellan optimal equiripple FIR filters [26]. The final stage can be reconfigured for spectroscopic analysis. By collecting frames at different passband FIR filters, spectroscopic images can be constructed relating information about reflected wavelengths.

2.3. State machine controller

On the FPGA, a finite state machine is in charge of hardware operation. It controls all FIFO's in and out of the FPGA. FIFO's carry initialization data from the host computer through the DSP, and acquisition data to the PC through the DSP. Also, the state machine is responsible for coefficients loaded to FIR filters; demodulation frequency, by means of a phase increment assigned to the quadrature mixer; X-galvo and Z-galvo (i.e. RSOD) waveform generation; and phase latencies due to transmission of controlling signals. The state machine ensures the dataflow is uninterrupted and uncorrupted.

2.4. Galvanometer waveform generation

Signals are generated for controlling each of the galvanometers used for fast X-Y scanning. The *X*-galvo is set up to increment upon the completion of a scan line. The increment amount is determined by a register, which is initialized at start up with a value correlated to the physical width to be scan.

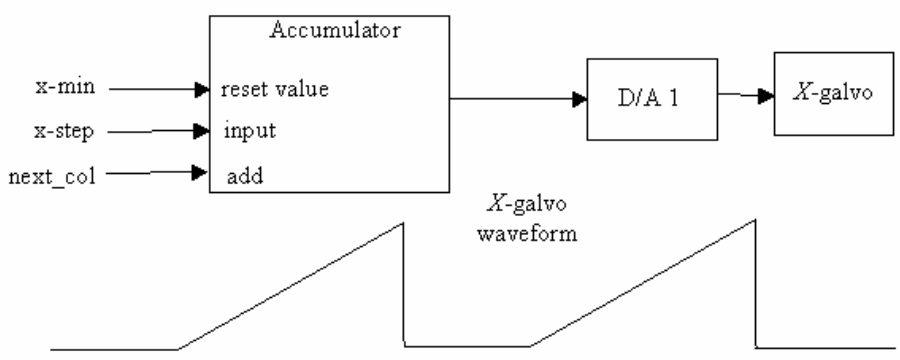

Figure 8. *X*-galvo hardware and a typical waveform.

The *Z*-galvo waveform controls the RSOD and is loaded into a RAM block. It has a trigger which signals to the finite state machine to begin scan line data acquisition. The frequency of the waveform is determined by the update counter reset threshold and the size number of values representing the waveform in the block RAM. This setup allows for easy configurability to each delay line used, whether the waveform is a 4KHz sinusoid, a 1KHz saw tooth, or any some other waveform.

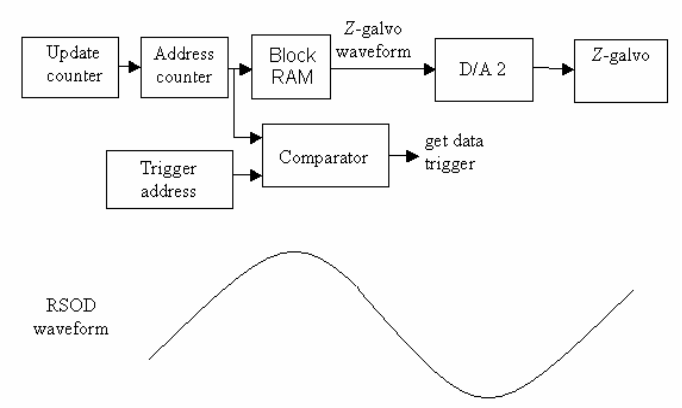

Figure 9. *Z*-galvo hardware and a typical RSOD sinusoid waveform.

2.5. DSP module

The DSP processor is a TI C6701 floating-point processor operating at 132 MHz. It has a pipelined, very long instruction word (VLIW) architecture that can execute up to eight instructions per clock cycle. The calculations performed on each sample are magnitude equal to $(Re^2 + Im^2)^{1/2}$ and phase equal to arctan(Im/Re). Arctan values are made available via a cache look-up table. By making the table eight way symmetric, high resolution is possible with reduced table size. The magnitude data represents the structural/spectroscopic OCT image. Taking the difference between two consecutive phases and dividing by the sampling period will yield the instantaneous frequency necessary for Doppler frequency shift detection. At very low image intensities, frequency shift information is useless, and thus it is set to zero. The DSP controls the data sent to and from the PCI bus and the FPGA. This includes initialization data, activation data, and acquisition data.

2.6. System processing tests

System processing tests consisted of running a function generator into the A/D input and analyzing the resulting images. All of the following tests involved a linear frequency sweep of a sinusoid from 400kHz to 1.2MHz over the span of 40ms with an amplitude of 1V. The figure to the right of each image data is a plot of the horizontal cross section. This plot represents the frequency sweep versus amplitude of specific measurement.

The first test is to set the demodulation frequency to 800256Hz and analyze the passband of the system as configured for magnitude retrieval. Note that the resolution dictates the closest frequency to 800kHz to be 521 X 1536Hz = 800256Hz. As seen from Figure 10, the transition band between the passband and stopband is smooth and accurately represents a linear sweep. The peak amplitude represents the presence of the 800256Hz frequency.

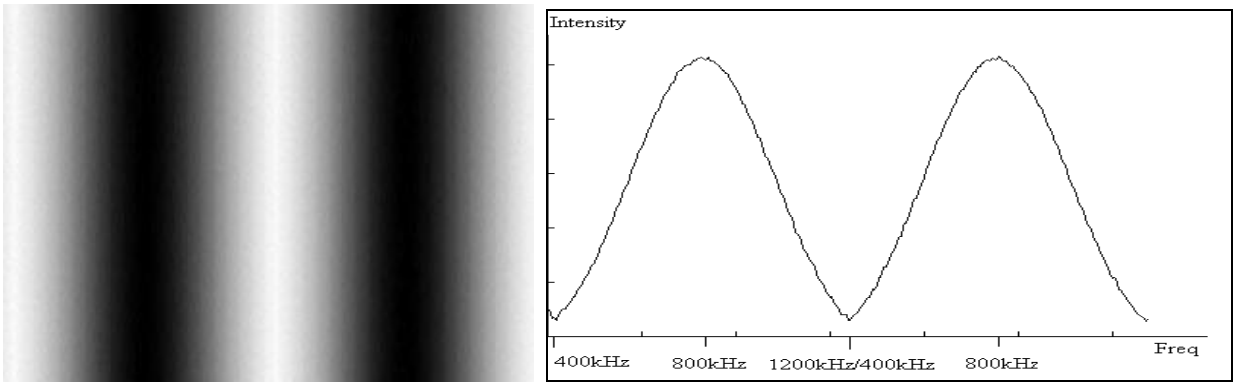

Figure 10. Image and cross-section of image for magnitude test of acquisition system with 800256Hz center frequency.

Next, to test the Doppler frequency shift detection ability of the system, the same demodulation frequency, 800256Hz, is used. The Doppler frequency shift is information in the phase of the interference data. Since the frequency sweep is linear, the expected shift detection shape is linear with a peak at 800256Hz. The downward slope corresponds to a velocity in the opposite direction. At the extremes, the plot is no longer smooth because the reduced image intensity corresponds to a reduced phase resolution.

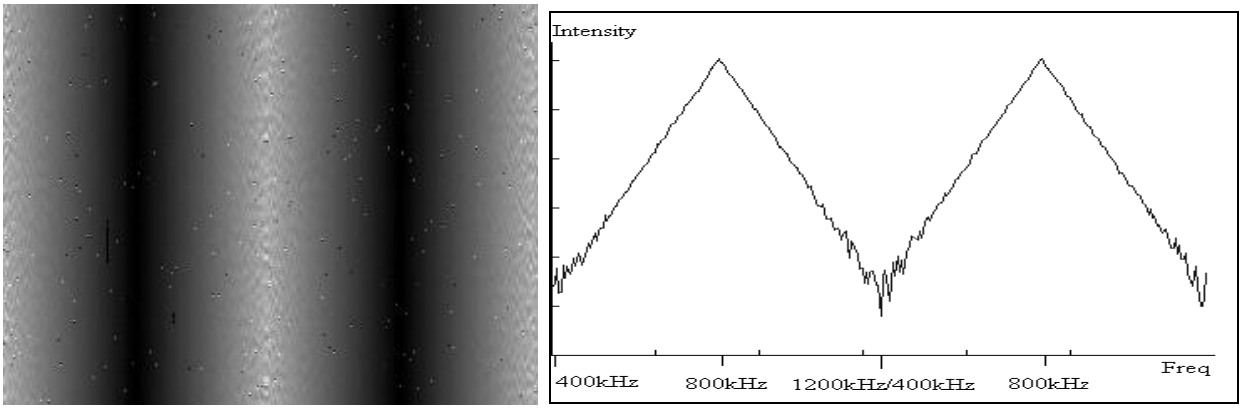

Figure 11. Image and cross-section of image for frequency shift detection test of acquisition system with 800256Hz center frequency.

Narrowband filters, useful for spectroscopic imaging, were tested with magnitude measurements. An image and cross-section for the frequency sweep with a demodulation frequency of 800256Hz is shown in Figure 12. This demonstrates the system's selectivity to a small bandwidth around the Doppler frequency.

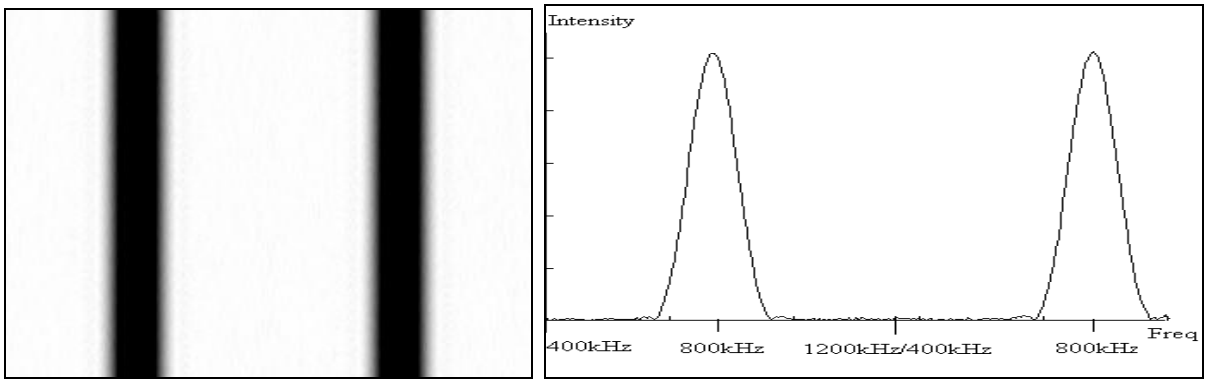

Figure 12. Image and cross-section of image for narrowband filtering tests of acquisition system with 800256Hz center frequency.

IMAGE ACQUISITION

For image acquisition, the OCT system optical source, a titanium:sapphire oscillator that pumps an ultra-high numerical aperture fiber broadens the spectrum of the laser to give approximately 60mW of power and a FWHM (full width half maximum) bandwidth of 100nm centered at 800nm.

Using a resonant RSOD driven by a sinusoid at 4 KHz, we acquired the cross-sectional images of a *Xenopus laevis* tadpole, as shown in Figure 13. The OCT images are an accumulation of 5 seconds of data captured at a rate of 4 frames per second and have a size of 0.5mm x 0.5mm (500X500 pixels) per frame. The Doppler frequency for this scan determined by the RSOD was 800kHz, thus we set the system's center demodulation frequency to be 800256Hz.

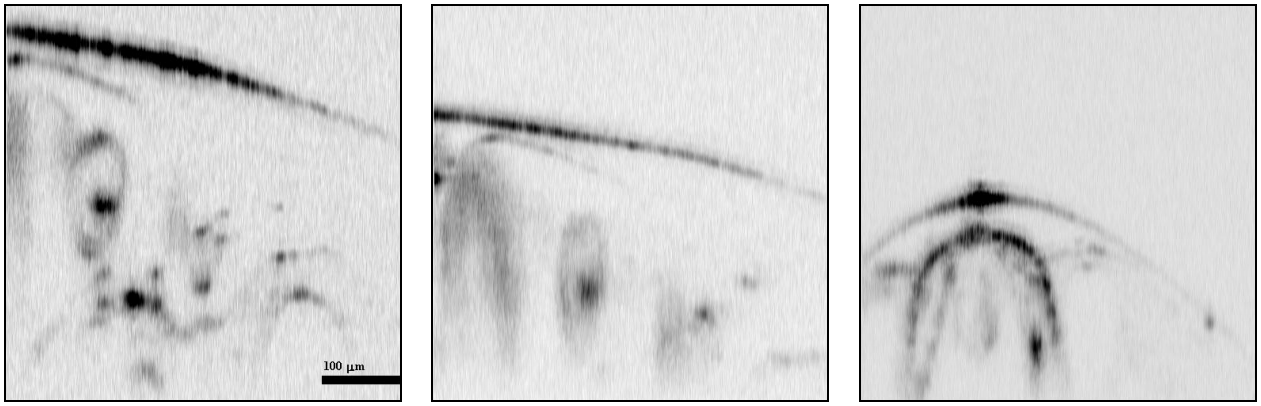

Figure 13. Fast scan OCT images of a *Xenopus laevis* tadpole. Images are an accumulation over duration of 5 seconds at 4 frames per second on the positive slope of a resonant RSOD.

The left and middle images show feature of the cardiovascular system, including a beating heart that was captured in real-time. The right image, acquired from the dorsal surface of the specimen, shows feature of the nervous system.

CONCLUSIONS

Outlined was our design for a highly configurable digital acquisition and processing system. The system can be reconfigured to operate with a variety of delay lines and at a wide range of modulation frequencies. The use of a tunable digital down converter allows for unique delay line based demodulation techniques. The unique FPGA design allows for real time processing of data for structural, Doppler and spectroscopic OCT imaging.

ACKNOWLEDGMENTS

This work was supported in part by the National Science Foundation (BES-0086696). We thank Jay Pasquesi for his work constructing our electrical circuits.

REFERENCES

1. D. Huang, E.A. Swanson, C.P. Lin, J.S. Schuman, W.G. Stinson, W. Chang, M.R. Hee, T. Flotte, K. Gregory, C.A. Puliafito, and J.G. Fujimoto, "Optical coherence tomography," *Science*, vol. 254, pp. 1178-1181, 1991.

2. G. J. Tearney, M. E. Brezinski, B.E. Bouma, S. A. Boppart, C. Pitris, J. F. Southern, and J. G. Fujimoto, "*In vivo* endoscopic optical biopsy with optical coherence tomography," *Science*, vol. 276, pp. 2037-2039, 1997.
3. J. A. Izatt, M. D. Kulkarni, S. Yazdanfar, J. K. Barton, and A. J. Welch, "*In vivo* bidirectional color Doppler flow imaging of picoliter blood volumes using optical coherence tomography," *Optics Letters*, vol. 22, no. 18, pp. 1439-1441, September 1997.
4. Z. Chen, Y. Zhao, S. M. Srinivas, J. S. Nelson, N. Prakash, and R. D. Frostig, "Optical Doppler Tomography," *IEEE Journal of Selected Topics in Quantum Electronics*, vol. 5, no. 4, pp. 1134-1141, July/August 1999.
5. A.V. Zvyagin, J.B. FitzGerald, K.K.M.B.D. Silva, and D.D. Sampson, "Real-time detection technique for Doppler optical coherence tomography," *Optics Letters*, vol. 25, no. 22, pp.1645-1647, November 2000.
6. Y. Zhao, Z. Chen, C. Saxer, S. Xiang, J. F. de Boer, and J. S. Nelson, "Phase-resolved optical coherence tomography and optical Doppler tomography for imaging blood flow in human skin with fast scanning speed and high velocity sensitivity," *Optics Letters*, vol. 25, no. 2, pp. 114-116, January 2000.
7. Z. Ding, Y. Zhao, H. Ren, J. S. Nelson, Z. Chen, "Real-time phase-resolved optical coherence tomography and optical Doppler tomography," *Optics Express*, vol. 10, no. 5, pp. 236-243, February 2002.
8. V. Westphal, S. Yadanfar, A.M. Rollins, and J.A. Izatt, "Real-time, high velocity-resolution color Doppler optical coherence tomography," *Optics Letters*, vol. 27, no. 1, January 2002.
9. Y. Zhao, Z. Chen, Z. Ding, H. Ren, and J.S. Nelson, "Real-time phase-resolved functional optical coherence tomography by use of optical Hilbert transform," *Optics Letters*, vol. 27, no. 2, pp.98-100, January 2002.
10. S. Yan, D. Piao, Q. Zhu, "DSP-based optical Doppler tomography system for real-time signal processing," *SPIE Bios 2003*, 4956-33, session 7, January 2003.
11. A.W. Schaefer, J.J. Reynolds, D.L. Marks, S.A. Boppart. "Real-time digital signal processing-based optical coherence tomography and Doppler optical coherence Tomography,". *IEEE Transactions on Biomedical Engineering*, 51(1):186-190, January 2004.
12. U. Morgner, W. Drexler, F.X. Kartner, X.D. Li, C. Pitris, E.P. Ippen, J.G. Fujimoto, "Spectroscopic optical coherence tomography," *Optics Letters*, vol. 25, no. 2, pp. 111-113, January 2000.
13. R. Leitgeb, M. Wojtkowski, A. Kowalczyk, C.K. Hitzenberger, M. Sticker, A.F. Fercher, "Spectral measurement of absorption by spectroscopic frequency-domain optical coherence tomography," *Optics Letters*, vol. 25, no. 11, pp. 820-822, June 2000.
14. D. J. Faber, E. G. Mik, M. C. G. Aalders, T. G. van Leeuwen, "Light absorption of (oxy-)hemoglobin assessed by spectroscopic optical coherence tomography." *Optics Letters*, vol. 28, no.16, pp. 1436-1438, August 2003.
15. B. H. Park, M. C. Pierce, B. Cense, J. F. de Boer, "Real-time multi-functional optical coherence tomography," *Optics Express*, vol. 11, no. 7, pp. 782-793, April 2003.
16. B. R. White, M.C. Pierce, N. Nassif, B. Cense, B. H. Park, G. J. Tearney, B. E. Bouma, T. C. Chen, J. F. de Boer, "*In vivo* dynamic human retinal blood flow imaging using ultra-high-speed spectral domain optical Doppler tomography," *Optics Express*, vol. 11, no. 25, pp. 3490-3497, December 2003.
17. V.X.D. Yang, M.L. Gordon, B. Qi, J. Pekar, S. Lo, E. Seng-Yue, A. Mok, B.C. Wilson, I.A. Vitkin, "High speed, wide velocity dynamic range Doppler optical coherence tomography (Part I): System design, signal processing, and performance," *Optics Express*, vol. 11, no. 7, pp. 794-809, April 2003.
18. J.F. de Boer, C.E. Saxer, J.S. Nelson, "Stable carrier generation and phase-resolved digital data processing in optical coherence tomography," *Applied Optics*, vol. 40, no. 31, pp. 5787-5790, November 2001.
19. G. J. Tearney, B. E. Bouma, and J. G. Fujimoto, "High-speed phase- and group-delay scanning with a grating-based phase control line," *Optics Letters*, vol. 22, no. 23, pp. 1811-1812, December 1997.
20. A. M. Rollins, M. D. Kulkarni, S. Yazdanfar, R. Ung-arunyawee, and J. A. Izatt, "In vivo video rate optical coherence tomography," *Opt. Express* ***3***, 219-229 (1998).
21. A.L. Oldenburg, J.J. Reynolds, D. L. Marks, and S. A. Boppart, "Fast-Fourier-domain delay line for in vivo optical coherence tomography with a polygonal scanner," Applied Optics, vol. 42, no. 22, pp. 4606-4611, August 2003.
22. P. Warnes, HEPC8 Full Length PCI HERON Module Carrier User Manual, Hunt Engineering Ltd., 1999.
23. P. Warnes, Hunt Engineering HERON-IO2 HERON Module with 200K/1M gate FPGA and 2 Channels of 105-MHz 12-bit A/D and 2 Channels of 125-MHz 14-bit D/A, Hunt Engineering Ltd., 2001.
24. M. Siggins and P. Warnes, HERON4 HERON processing module for C6201 & C6701, Hunt Engineering Ltd., 1999.
25. Xilinx Inc., Direct Digital Synthesizer (DDS) v4.1 Product Specification, 2001.
26. Programs for Digital Signal Processing, IEEE Press, New York, 1979, Algorithm 5.1.